Using acetowhite opacity index for detecting cervical intraepithelial neoplasia

Wenjing Li
Sankar Venkataraman
Ulf Gustafsson
Jody C. Oyama
STI Medical Systems
733 Bishop Street
Honolulu, Hawaii 96813

Daron G. Ferris
Medical College of Georgia
Department of Family Medicine
and Obstetrics and Gynecology
Augusta, Georgia 30912

Rich W. Lieberman
University of Michigan Medical School
Department of Pathology and Obstetrics
and Gynecology
Ann Arbor, Michigan 48109

Abstract. Cervical intraepithelial neoplasia (CIN) exhibits certain morphologic features that can be identified during a colposcopic exam. Immature metaplastic and dysplastic cervical squamous epithelia turn white after application of acetic acid during the exam. The whitening process occurs visually over several minutes and subjectively helps to discriminate between dysplastic and normal tissue. Digital imaging technologies enable us to assist the physician in analyzing acetowhite (acetic-acid-induced) lesions in a fully automatic way. We report a study designed to measure multiple parameters of the acetowhitening process from two images captured with a digital colposcope. One image is captured before the acetic acid application, and the other is captured after the acetic acid application. The spatial change of the acetowhitening is extracted using color and texture information in the post-acetic-acid image; the temporal change is extracted from the intensity and color changes between the post-acetic-acid and pre-acetic-acid images with an automatic alignment. In particular, we propose an automatic means to calculate an opacity index that indicates the grades of temporal change. The imaging and data analysis system is evaluated with a total of 99 human subjects. The proposed opacity index demonstrates a sensitivity and specificity of 94 and 87%, respectively, for discriminating high-grade dysplasia (CIN2+) from normal and low-grade subjects, considering histology as the gold standard.
[DOI: 10.1117/1.3079810]

Keywords: digital colposcopy; image analysis; cervical neoplasia; acetowhite; computer-aided diagnostic; opacity index.

Paper 08295R received Aug. 25, 2008; revised manuscript received Dec. 11, 2008; accepted for publication Dec. 19, 2008; published online Feb. 19, 2009.

1 Introduction

Cervical neoplasias exhibit certain morphologic features that can be identified during a colposcopic examination. These features include distinct epithelial and vascular abnormalities. Acetowhite epithelium is one of the major colposcopic signs observed in cervical neoplasia. Although acetowhite epithelium does not universally equate with neoplastic tissue,[1] virtually all cervical neoplasias display a variably transient and opaque white color following the application of 3 to 5% acetic acid. Consequently, colposcopic indices consider acetowhite epithelium to help predict the severity of cervical lesions.[2]

Colposcopy is the primary diagnostic tool for identifying the most atypical sites for biopsy of the cervix, following an abnormal cytological screening (Pap smear). However, due to the subjective nature of the examination, the accuracy of colposcopy is highly dependent on colposcopists' experience and expertise. It has been estimated that approximately one third of high-grade disease is missed by initial colposcopy.[3] The advent of digitized medical images has led to an increasingly important and evolving role for image processing and computer-aided diagnostic (CAD) systems. An automated image analysis system of uterine cervical images could provide the means for the identification and analysis of diagnostic features from cervical images, and ultimately, derive a clinical diagnosis following an objective and quantifiable process.

Automated detection of acetowhite epithelium depicted on cervical images has been a challenging task due to light reflection, various amounts of illumination, and wide inter- and intrapatient variation. A small number of automated detection studies have been conducted. Most of these studies have focused on the segmentation of acetowhite epithelium. Yang et al. developed a sophisticated technique for detection of acetowhite epithelium using *K*-means clustering and a deterministic annealing technique.[4] Gordon and her coworkers developed an unsupervised segmentation algorithm for three tissue types in cervical imagery using a Gaussian mixture model.[5] In their latest work,[6] the acetowhite region was identified by extracting the highest mean intensity cluster among the smooth regions. They also noted that due to illumination effects and large intrapatient variation, acetowhite lesions are incorrectly detected. Additionally, acetowhite lesions located in shaded areas of the image are not detected at all. The work

Address all correspondence to: Wenjing Li, PhD, STI Medical Systems, 733 Bishop Street, Honolulu, HI, 96813. Tel: 808-540-4768; Fax: 808-540-4850; E-mail: wli@sti-hawaii.com.

1083-3668/2009/14(1)/014020/10/$25.00 © 2009 SPIE

just referenced was based on Cervigram™ images collected by the National Cancer Institute, and limited to one image per subject.

One pioneering study by Pogue et al.[7] evaluated different metrics of the region of interest in cervical images and indicated that computer-based processing of cervical images can provide some discrimination of tissue features that could be useful for clinical evaluation. Specifically, it was mentioned that the Euler number could be used as a clinical feature to discriminate metaplasia from neoplasia. The study was done semiautomatically using Adobe Photoshop software and MATLAB (The MathWorks Inc., Natick, Massachusetts) using a small number of human subjects (nine subjects).

Researchers have also been focusing on using the temporal evolution of the tissue changes for discrimination of cervical neoplasia. Pogue et al.[8] analyzed the time sequence data of cervical intraepithelial neoplasia of grades 2 and 3 (CIN2/3) and normal mature squamous epithelium captured after application of acetic acid every 20 s for up to 10 min decay. It was concluded that the normalized green to red ratio where the data are time averaged over a 100-s interval provided a robust method to distinguish mature squamous epithelium for CIN2/3 in a small data set of six human subjects. Studies by Balas et al.[9] and Balas[10] indicate that the intensity of the backscattered light captured at 550 ± 25 nm during the decay sequence can be used to improve the sensitivity and specificity of the *in vivo* diagnosis. Kaufman et al.[11] at MediSpectra, Inc., filed a patent on analyzing the intensity changes of the decay sequence and indicated the ratio of mean values of Green/Red) from two time intervals (100 to 200 s) and (200 to 300 s) can be used to discriminate CIN2/3 lesions from normal and CIN1 lesions. The region of interest in these studies was manually marked, and image registration was not addressed or handled semiautomatically. One recent publication[12] reveals a performance with sensitivity and specificity of 79 and 88% to differentiate high-grade intraepithelial lesions from normal or low-grade intraepithelial lesions using 29 patients. Statistical learning algorithms including *K*-nearest neighbor (KNN) and support vector machine (SVM) were applied on the white light reflectance images to capture the acetowhite changes by selecting features such as intensities of red, green, and blue channels and ratios of intensities.

The purpose of this study is to explore a fully automated color imaging system to analyze acetowhite lesions. We present the use of a digital colposcope, which acquires polarized and nonpolarized color cervical images during a clinical exam. A sequence of image-processing algorithms is used to analyze the anatomic interests of the cervix, extract the color and opacity property of the acetowhite epithelium, and locate acetowhite lesions. In particular, we present automatic means to calculate an opacity index, which indicates the grades of temporal change. The system was evaluated with 99 human subjects and demonstrates a good correlation with pathology-confirmed lesions. A sensitivity and specificity of 94 and 87% was achieved for discriminating high-grade (CIN2+) lesions from normal and low-grade lesions using automated extracted opacity index parameters.

2 Materials and Methods

2.1 *Clinical Examination*

Women 22 to 50 years old (with an average age 35 ± 7.8; 28 women were in their twenties, 40 were in their thirties, 30 were in their forties, and one woman was 50) with previously detected abnormal cervical cytologic abnormalities, a concordant colposcopic diagnosis, and scheduled for an electrosurgical loop excision procedure were asked to enroll in the trials conducted at hospitals in Lima and Cusco in Peru, and in Augusta, Georgia, USA. All subjects read and signed an institutional-review-board-approved informed consent document. Among the study subjects, 10 were menopausal; the other subjects were all premenopausal. The study protocol and the informed consent form for the Peru trial were approved by the Institutional Review Board (IRB) at the Instituto Especializado de Enfermedades Neoplasicas (Mite Revisor de Protocolos de la Oficina Ejecutiva de Apoyo a la Investigacion ye Docencia Especializado), and by the hospital Ethics Committee (Comite de Etica). The IRB approval for the Augusta study was conducted through the Clinical Investigation Regulatory Office, Department of the Army, Fort Sam Houston. Subject confidentiality was protected and no identifying subject information was recorded for the study. Exclusion criteria included cervical hemorrhage, pregnancy, and unwillingness to participate. Image data from 99 subjects were used in the assessment of the automated image analysis system.

Prior to application of 5% acetic acid, polarized and nonpolarized high-resolution digital cervical RGB images were taken of the ectocervix. The solution of 5% acetic acid was applied with solution-soaked cotton balls placed in contact with the surface of the cervix for 1 min. Polarized and nonpolarized cervical pictures were taken 1 min after the acetic acid application. Thereafter, following Lugol's iodine solution application, another set of polarized and nonpolarized images were acquired. After application of Lugol's iodine, subcutaneous administration of an anesthetic and vasoconstrictive agent, and electrosurgical loop excision or conization were performed, as necessary. Proper orientation was maintained between the ectocervix and specimen. Final post surgical polarized and nonpolarized images of the ectocervix and a single nonpolarized image of the excised specimen were then obtained.

The specimen was sent to a pathology laboratory (Mlabs, University of Michigan, Ann Arbor) for histological analysis. Histopathologic diagnoses were rendered from annotations of serially sectioned loop excision specimens obtained from the same subject. For a subset of patients, the bread-loaf-sectioned loop excision tissue was examined by pathologists to render a histologic "map" of the loop excision specimen. The histological map provides detailed diagnostic information according to normal, low-grade squamous intraepithelial lesion (LSIL), and high-grade squamous intraepithelial lesion (HSIL) and invasive cancer. The histological map was presented as projected lines on a colposcopic image to generate a pathology-based criterion standard. If possible, HSIL were further classified as CIN2, CIN23, or CIN3 by pathologists. A sample histological map is presented in Fig. 8(d) in Sec. 3.

A subset of the cervical images acquired was also evaluated by an expert colposcopist. Colposcopic features including ectocervix, external os, columnar epithelium, squamous

Fig. 1 High-resolution digital colposcope with polarized imaging capability.

epithelium, and acetowhite epithelium were annotated using a computer-based drawing program (Photoshop CS2, Adobe System Inc., San Jose, California). A sample annotated colposcopic image is displayed in Fig. 3(b) in Sec. 2.3.1. The colposcopic image annotation served as the ground truth information for the colposcopic feature extraction during the algorithm development.

2.2 *Digital Colposcope*

As a potential source of high-resolution digital imagery for colposcopy, Science and Technology International's (Honolulu, Hawaii) digital colposcope was developed to acquire images with a resolution sufficient for vessel detection. The digital colposcope, as seen in Fig. 1, utilizes a standard colposcope (Seiler, Series 935), two high-resolution 14-Mpixel digital cameras (Kodak, DCS Pro SLR/n), and a fiber-guided light source assembly (Perkin Elmer, DiX1765 xenon lamp). In addition to high-resolution imaging capabilities, the digital colposcope includes stereoscopic imaging capabilities (which can be used for 3-D image reconstruction) and polarized image acquisition (used to reduce glare). The images acquired were stored in Digital Camera Raw (DCR) format with no compression and later converted to tagged image file format (TIFF) automatically prior to the application of image processing algorithms. In our system, 92 pixels represent 1 mm, a resolution that can enable computer programs to detect fine and coarse mosaic, punctation, and atypical blood vessels and assess intercapillary distances. An important feature of our digital colposcope is the inclusion of polarization, which reduces obscuring glare that may be misinterpreted as acetowhite epithelium.

A calibration unit is part of the digital colposcope setup and is used to acquire calibration data at the clinic sites. The calibration is performed daily before subject examinations. The purpose of calibration is to ensure that images acquired at different times and with different colposcopes exhibit identical intensity and color values, independent of camera/camera settings and the light source used. This can be achieved by mapping the color appearance of the image taken with different instruments into a standard color space. The details of the image calibration procedure can be found in a previous published paper.[13]

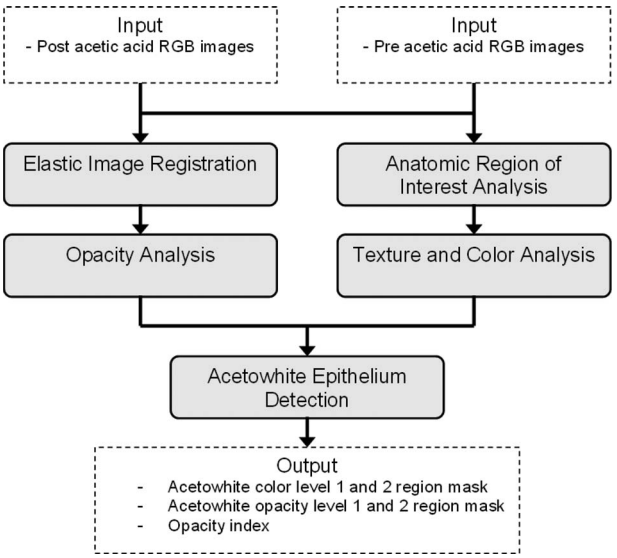

Fig. 2 Flowchart of automated image analysis.

2.3 *Automated Image Analysis*

We developed an automated image analysis system to identify unique cervical features with an initial goal to identify normal cervical anatomy and acetowhite epithelium. To characterize both color and opacity property of acetowhite epithelium, images before and after acetic acid application are required. A multistep procedure (Fig. 2) using a set of image-processing algorithms is utilized to analyze the acetowhite epithelium.

In our analysis, the post-acetic-acid image is used as the reference image. The post-acetic-acid image is first analyzed with regard to the anatomy of the cervix to identify the cervix, cervical os, and columnar epithelium. The next step in the post-acetic-acid image analysis is to extract the color and spatial property of the acetowhite epithelium. To address the opacity property of acetowhite epithelium, the pre- and post-acetic-acid images are accurately registered using an elastic image registration algorithm. By subtracting the registered pre-acetic-acid image from the post-acetic-acid image and applying unsupervised clustering algorithms, the opacity property of the acetowhite epithelium can be determined. An opacity index is then computed based on the clustering results. The details of the image analysis are described in the following subsections.

2.3.1 *Anatomical region of interest analysis*

The anatomical region of interest analysis is a fully automated procedure and detects the cervix, cervical os, and columnar epithelium in the sequential order. To ensure that an image of the entire cervix is acquired, the magnification level of the colposcope is selected such that the cervical image also contains the edge of the speculum and the vaginal wall. Prior to any further image processing, the cervix region must, thus, be extracted as the region of interest. The main challenge in finding the cervix region is excluding the vaginal wall as its texture and color mimic that of cervical squamous and mature metaplastic epithelia. Our implementation of a fully automatic cervix region detection algorithm uses an unsupervised two-class clustering technique based on GMM (Gaussian mixture

model). Unlike previously published work,[6] we do not assume that the cervix region is preferably located in the center of the image.

The details of the cervix region detection algorithm are as follows. First, a Gaussian smoothing function[14] is applied to the RGB image of the cervix to reduce the amount of noise. Second, the Karhunen-Loeve (K-L) transformation is applied to transform the image from RGB color space into K-L space. The K-L space has proved to be a very effective color space for color-texture characterization in the analysis of skin lesions[15] and in colon tumor detection.[16] Third, the expectation maximization (EM) algorithm[17,18] is used to cluster the K_1 channel (the eigenvector corresponding to the largest eigenvalue during eigendecomposition) as foreground and background. The EM algorithm is used for cervix region detection because it has been shown to provide a robust segmentation result for a two-class image segmentation problem and because it does not require any parameters. Fourth, within the foreground region, the vaginal folds are first detected using color and gradient information, and then polynomial curves are fitted using the detected data points to extend the vaginal folds to the foreground boundary. The vaginal regions are defined as the cutout areas from the foreground region using the fitted curves.[19]

The cervical os defines the portion of the cervical canal that is covered by the columnar epithelium. If visible, the cervical os is usually a small-area region located in the center of the cervix with low intensity, surrounded by the columnar epithelium and the transformation zone (TZ). The os region detection algorithm is based on mean shift clustering,[20,21] given the assumption that the os region is probably located in the center portion of the detected cervical region with the lowest intensity, not the simple image center. The mean shift algorithm is a nonparametric clustering technique that does not require prior knowledge of the number of clusters, and does not constrain the shape of the clusters. It is based on kernel density gradient estimation theory and is guaranteed to converge to a point where the gradient of the density function is zero. As already indicated, the reasons for applying the mean shift clustering algorithm for os detection are that (1) it does not require a preset the number of clusters and (2) the segmentation is not very sensitive to the choice of resolution parameters.[21]

The os detection algorithm is applied to the cervix region only and starts by computing a distance transform[22,23] to create a distance image. The distances are calculated based on a Euclidean metric. The purpose of the distance image is to locate the center portion of the cervical region. In the second step, mean shift clustering is applied on the preselected search range of the K_1 channel of the image. The cervical os region is then obtained by selecting the cluster with lowest intensity, followed by morphological operations to remove small noisy regions. To improve the robustness of the os detection, the os detection algorithm is applied three times with three different search range parameters defined as $\frac{1}{4}$, $\frac{1}{2}$, and $\frac{3}{4}$ of the cervix region area. The final os region is the os region with maximal area value.

The columnar region appears reddish even after application of acetic acid. This color information is crucial in segmenting the columnar region. The columnar detection algorithm applies the mean shift algorithm to segment the columnar region.

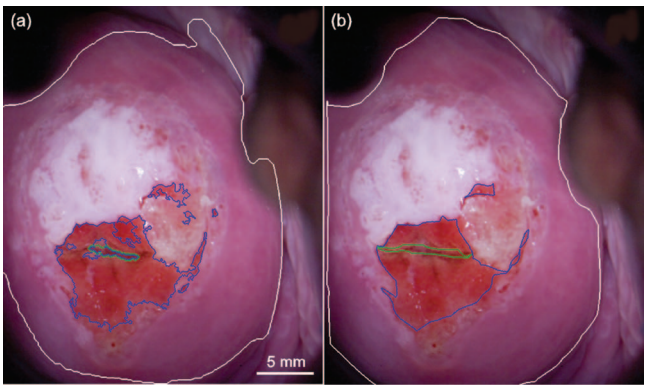

Fig. 3 Example of extracting anatomical features of interests in cervical images: white outline, cervix region; green; cervical os region; and blue; columnar epithelium. (a) Algorithm results, and (b) annotation by expert colposcopist.

An example of the anatomic region of interest detection result can be found in Fig. 3(a). For comparison, the corresponding doctor's annotation can be found in Fig. 3(b). In these figures, the cervix region is outlined by a white contour, the cervical os region is indicated by a green contour, and the columnar epithelium is outlined by blue contours.

2.3.2 *Acetowhite texture and color analysis*

Given one post-acetic-acid image, acetowhite epithelium can be assessed by its visual characteristics with respect to texture and color. The following steps are applied in the analysis of the texture and color properties of acetowhite lesions.

Step 1: Texture region extraction. Given the normal anatomy regions in a cervical image, excluding the os region and columnar epithelium region from the cervix region, a region containing squamous epithelium, metaplastic, and dysplastic tissue is obtained. In this first step, the focus is on extracting regions exhibiting a high degree of texture independent of the color information. Here, the texture analysis is a way to quantify properties described in terms of rough, smooth, silky, or bumpy as a function of the spatial intensity variations in an image. In a sense, the roughness or bumpiness refers to the variations in intensity values, or gray levels. For the cervix, this texture is an important visual cue in identifying the vasculature and gland openings from the surrounding homogeneous squamous tissue. The texture region is served as one important region of interest for the acetowhite region detection. When acetowhite region is accompanied with a large area of vascular patterns, segmenting by color property only does not yield ideal results. A combination of texture and color analysis is preferred to segment the acetowhite regions.

The technique presented in Refs. 24–26 is used to extract the texture features in the image. The texture features used describe both the underlying texture parameters and the adequate texture scale. The width of a Gaussian window defines the scale of the texture features. The second-moment matrix for the gradient vectors within this window, computed for each pixel in the image, can be approximated using

$$\mathbf{M}_{\sigma}(x,y) = G_{\sigma}(x,y)^{*}(\nabla I)^{*}(\nabla I)^{T} \quad (1)$$

where G_{σ} is a separable binomial approximation to a Gaussian smoothing kernel with variance σ^2, and (∇I) is the gradient of the image intensity. At each pixel location, $\mathbf{M}_{\sigma}(x,y)$ is a 2×2 symmetric positive semidefinite matrix. The trace of the matrix yields the total energy of the image function at (x,y), the edge busyness, which can be used for measuring the homogeneity of segment-type features. We refer the trace of the second-moment matrix as texture contrast, which can be computed according to

$$\text{contrast} = (\lambda_1 + \lambda_2)^{1/2}, \quad (2)$$

where λ_1 and λ_2 are the eigenvalues of $\mathbf{M}_{\sigma}$.

The texture region is then obtained by applying the two-class EM clustering algorithm in the texture feature space. The texture region detected for the cervical image in Fig. 3(a) is shown as white regions in the binary image of Fig. 5(a) in the discussion of step 3.

Step 2: Color region extraction. Color is the major image property used to distinguish acetowhite lesions from normal mature squamous epithelium, which appears as pinkish color in cervical images. In this second step of the texture and color analysis, we focus on color information only, and the region of interest is the cervix region excluding the os region, columnar epithelium region, and texture region determined in the first step.

The rationale for excluding the texture region from the color analysis is that when abnormal vasculature is overlaid on the acetowhite region, the acetowhite color information is going to be "degraded" or "less white" due to the larger amount of red blood vessels. We have found that excluding the texture regions from the acetowhite color analysis and combining the color and texture regions later will yield a more consistent result over the entire data set when comparing to the colposcopic annotations.

The region of interest in this step exhibits a near homogenous surface and usually consists of normal mature squamous epithelium and/or an acetowhite region. The intent of this step is to extract the acetowhite lesions from the squamous epithelium. A method previously described by Li et al.[27] is utilized. This method uses the number of dominant peaks in the RGB G channel histogram to deduce the information about the size of the acetowhite region and what method should be used in the subsequent segmentation step. A one-peak histogram is indicative of a small acetowhite region, whereas a two-peak histogram indicates a large homogeneous acetowhite region. Segmentation of the region of interest is accomplished by the mean shift clustering algorithm for a one-peak histogram and by the EM algorithm for a two-peak histogram. For the subject shown in Fig. 3, a two-peak histogram is obtained for the homogenous cervical tissue region. This two-peak histogram is shown in Fig. 4(a) and the corresponding segmentation according to mature squamous tissue (white) and acetowhite tissue (gray) using the EM algorithm is displayed in Fig. 4(b).

Step 3: Combining color and texture. By combining the color and texture information obtained in steps 1 and 2, a candidate acetowhite epithelium region, as illustrated in Fig. 5(b), is obtained. This entire color and texture region is further analyzed based on its color properties using the CIE-*Lab* color space due to its perceptual uniformity. The three parameters in the CIE-*Lab* color space represents the luminance of the color (L), its position between red and green (a), and its position between yellow and blue (b). The nonlinear relations for L, a, and b are intended to mimic the logarithms response of the human eye.[28]

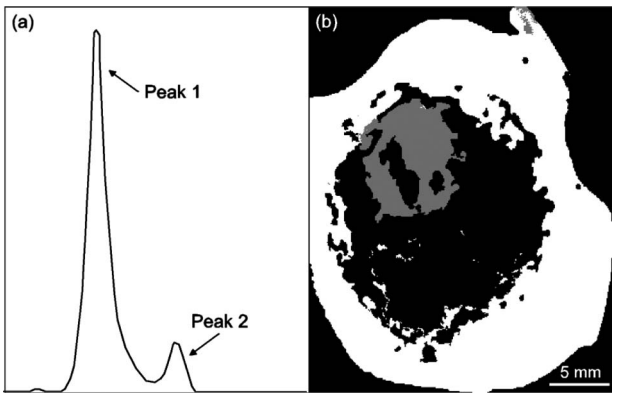

Fig. 4 Acetowhite color region extraction: (a) two-peak intensity histogram of homogenous cervical tissue, and (b) the homogenous tissue are segmented as acetowhite region (gray) and mature squamous region (white) using color information. The dark region within the cervix region corresponds to the cervical os, columnar epithelium, and the texture region.

To match the colposcopic annotations with the terms of "opaque white," "intermediate opaque white," and "translucent white," a three-class K-means algorithm[29] is applied to classify the candidate region into three levels of whitish regions. These regions are sorted according to their color scores computed according to

$$\text{score}(i) = \begin{cases} (a_i - a_{\text{sq}})^2 + (b_i - b_{\text{sq}})^2, & \text{if } a_i \leqslant a_{\text{sq}} \\ -[(a_i - a_{\text{sq}})^2 + (b_i - b_{\text{sq}})^2], & \text{if } a_i > a_{\text{sq}} \end{cases}, \quad (3)$$

where a_i and b_i indicate the average values of the a and b channels, respectively, for the corresponding whitish region i (=1,2 3), and a_{sq} is the mean a channel value of the mature squamous epithelium region in the image. The mature squamous epithelium region is obtained by excluding the os, columnar epithelium, and the combined texture and color region from the cervix region.

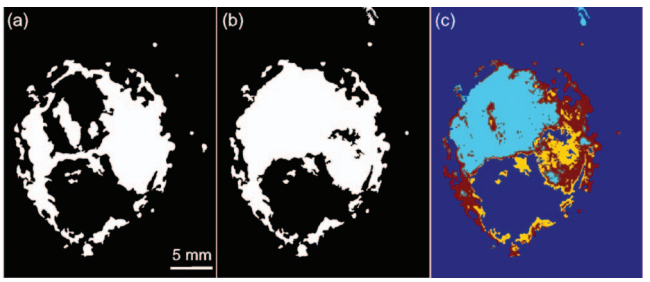

Fig. 5 Acetowhite color analysis: (a) binary map of the texture region, (b) binary map of the combined texture and acetowhite color regions, (c) automatic three-level clustering using color information.

In our analysis, the higher the color score, the whiter the region appears. The result of the three-class clustering is shown in Fig. 5(c) with the light blue color indicating the highest color score, the dark red the middle color score, and yellow the lowest color score. The yellow region is considered metaplastic region instead of acetowhite lesion due to its low-color score.

2.3.3 *Elastic image registration*

In colposcopy, acetowhite epithelium refers to epithelium that transiently changes color from pink or red to white after the application acetic acid. One limitation of the texture and color analysis of the post-acetic-acid image only is that we can only assess the property of acetowhite epithelium spatially. To determine how much the color and intensity changes by the acetic acid application, we should also analyze the image of the cervix acquired before applying acetic acid.

An important step prior to the opacity analysis is to align, or register, the pre- and post-acetic-acid images. For the acetic acid application method applied in our clinical trials in Peru and the United States, it usually takes 1 to 2 min for the acetic acid to take effect. During this time, relatively large movements of the patient, device, and tissue can occur. Registration methods based on geometric features[30] usually show poor performance for this case due to lack of robust features in the tissue images. To account for these movements, we developed a robust and fully automated elastic registration algorithm to register the pre- and post-acetic-acid images. The method is formulated as an optimization over a set of continuous deformation vector fields:[31,32]

$$h^* = \mathrm{argmin}_h[J(f,g,h)], \tag{4}$$

$$J(f,g,h) = J_D(f,g,h) + \alpha J_R(h), \tag{5}$$

where h^* is the optimal solution, f and g are the images to be registered, J_D is a cost function measuring the dissimilarity between the images, J_R is a regularization term, and α is a proportionality constant determining how much regularization is used.

The similarity is based on the normalized sum of the squared differences between the acetic acid image g and the pre-acetic-acid image f, deformed by h:

$$J_D(h,f,g) = \sum_{i,j} \{f[h(i,j) + (i,j)] - g(i,j)\}^2. \tag{6}$$

The regularization criterion J_R penalizes unsmooth deformations. We choose J_R so that its gradient coincides with the linearized 2-D elastic operator describing equilibrium in an elastic material.

$$\nabla J_R(h) = \xi \Delta h + (1-\xi)\,\nabla(\nabla \cdot h). \tag{7}$$

The ξ is a constant in the range of [0, 1]. By adding the regularization criterion to the global cost function, we model the image as an elastic sheet that tries to retain its form in the presence of an external force. The J_R can be expressed in the following discrete form

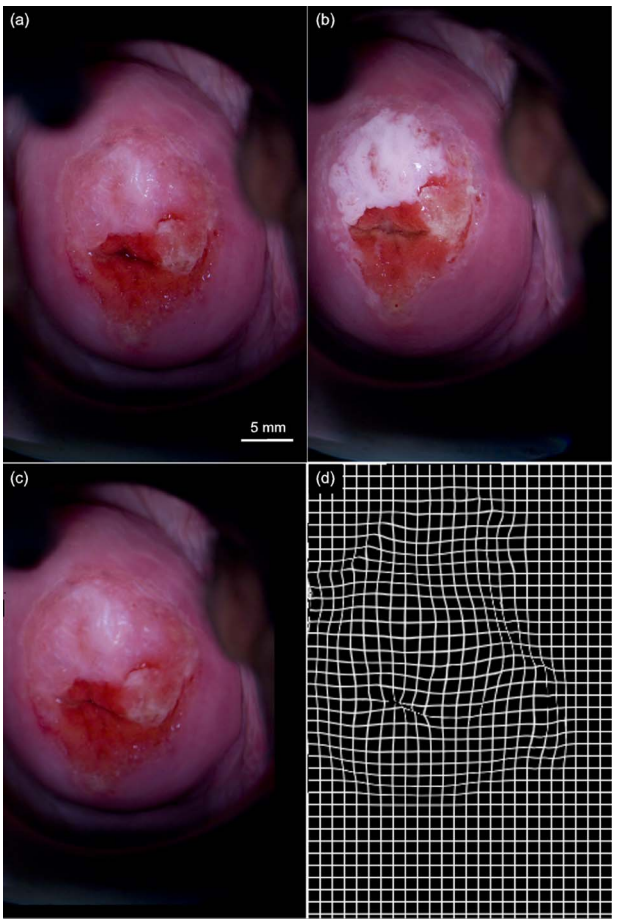

Fig. 6 Elastic image registration (a) pre-acetic-acid image, (b) post-acetic-acid image, (c) registered pre-acetic-acid-image, and (d) the display of soft tissue movement after translation.

$$J_R(h) = \sum_{i,j} \{\xi(\Delta_1 h^1_{i,j})^2 + (1-\xi)[(\Delta_1 h^1_{i,j})^2 + (\Delta_2 h^1_{i,j})^2]\} + \{\xi(\Delta_2 h^2_{i,j})^2 + (1-\xi)[(\Delta_2 h^2_{i,j})^2 + (\Delta_1 h^2_{i,j})^2]\}, \tag{8}$$

where

$$\Delta_1 h^k_{i,j} = h^k_{i,j} - h^k_{i-1,j}, \quad \Delta_2 h^k_{i,j} = h^k_{i,j} - h^k_{i,j-1}. \tag{9}$$

The initial transformation is assumed to be translation only. The translation vectors are calculated using the normalized 2-D cross-correlation. The method of gradient descent with adaptive step size is used for optimization. To speed up the transformation process, the multiresolution scheme is employed.

In our application, texture and color analysis is performed on the post-acetic-acid image. Our registration process is, thus, designed to deform the pre-acetic-acid image to fit the post-acetic-acid image. Figure 6 shows an example of registering a pre-acetic-acid image with a post-acetic-acid image. Figure 6(a) is the image of cervix before the acetic acid application, and Fig. 6(b) is the image after the acetic acid application. Figure 6(c) is the registered/aligned pre-acetic-acid image, and Fig. 6(d) is a display of the displacement of the vector fields after the translation, which demonstrates the local deformation of the tissue.

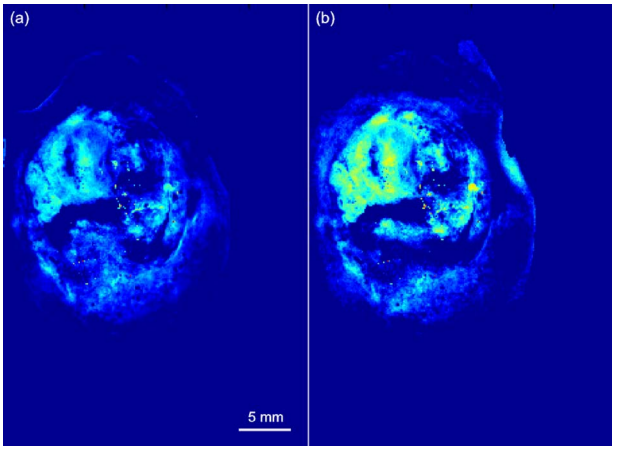

Fig. 7 Opacity analysis: (a) difference in G channel of RGB color space, and (b) difference in *a* channel of CIE-*Lab* color space.

2.3.4 *Acetowhite opacity analysis*

After image alignment, the acetic-acid-induced changes can be captured by subtracting the registered pre-acetic-acid image from the post-acetic-acid image. Figure 7(a) shows the difference of the two images in the G channel in RGB space and Fig. 7(b) shows the differences of the two images in the *a* channel in CIE-*Lab* space.

Immature metaplasia and columnar epithelium tissue also turns transiently white after acetic acid application. These epithelia do not exhibit dysplastic tissue changes and should be excluded from the acetowhite region of interest. Due to the fact that these tissue regions usually exhibit a minor opacity change, we apply a two-step mean shift clustering algorithm in the color difference feature space. The first step segments the dominant opacity change and removes minor opacity change. The second step segments the most opaque change from the foreground region obtained in the first step. An opacity index is computed as the mean color difference of the most opaque region. Here, the most opaque region is defined as the region with the largest mean color difference. The definition of the opacity index is as follows:

$$\text{OpacityIndex} = \frac{1}{(2^n - 1)\Omega}\left\{\sum_{i,j}[f_k^*(i,j) - g_k(i,j)]^p * r(i,j)\right\}^{1/p}, \tag{10}$$

where n is the number of bits of the image; f_k^* is the registered pre-acetic-acid image; and g_k is the selected post acetic acid image, both at the k color channel of the image ($k=1,2,3$); r is the most opaque region extracted from the mean shift clustering algorithm in binary form; Ω is the number of foreground pixels in the opaque region r. The p norm metric can be used but for simplicity, p is set to 1 in the current implementation.

Generally speaking, the opacity index determination can be applied to images in any color space. However, in the current implementation the *a* channel of the perceptually uniform CIE-*Lab* color space is utilized. Unlike the *L* channel, or red, green, and blue in RGB color space, the *a* channel is not affected by the light distribution and intensity of the light source. Also since the color of cervical tissue usually changes from pink/red to white after acetic acid wash, the *a* channel is chosen instead of the *b* channel to better capture the color changes of cervical tissue. The corresponding experimental results are described in the following section.

The final acetowhite epithelium is obtained by grouping the acetowhite color regions with similar opacity values. The postprocessing step is used to obtain more accurate lesion boundary using the spatial information from the texture and color analysis.

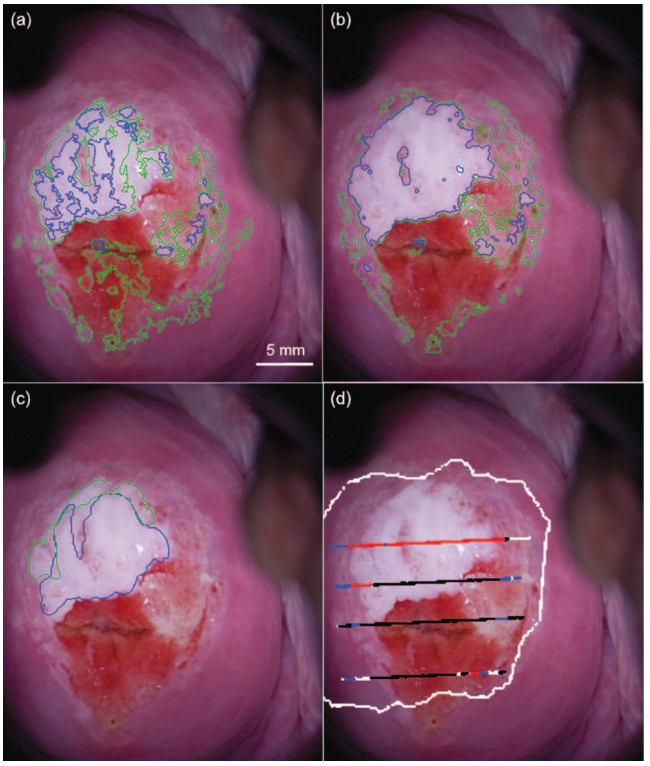

Fig. 8 (a) Acetowhite opacity analysis, blue-opaque, green-intermediate opaque; (b) final acetowhite epithelium detection, blue-first level of white, green-second level of white; (c) colposcopic annotations, blue-opaque white, green-intermediate opaque white, and (d) Histopathology results: white–normal; black–no epithelium/burned epithelium; blue–LSIL; red–HSIL.

3 Results

Figure 8 illustrates the acetowhite epithelium analysis results from one subject with HSIL. Figure 8(a) is the results overlay of the opacity analysis and regions with blue contours indicate the most opaque white lesions and regions with green contours are indicative of intermediate opaque white lesions. Figure 8(b) is the result of final acetowhite epithelium detection, which combines the texture and color analysis with the opacity analysis. The blue contours indicate the first level of acetowhite regions and the green contours outline the second level of acetowhite regions. By combining texture, color, and opacity, the different acetowhite regions now correlate well with the colposcopic annotations, as illustrated in Fig. 8(c). In Fig. 8(c) the colposcopic annotations of opaque white and intermediate-opaque white are indicated by blue and green outlines, respectively. Figure 8(d) is the histological map on

Table 1 Performance of image analysis systems compared with colposcopic annotations.

Cervical Features	PPA (%)	NPA (%)
Cervix	86.2	95.7
Cervical os	46.0	99.2
Columnar epithelium	68.1	96.8
Acetowhite epithelium	65.0	90.1

the cervical image. The white outline indicates the contour of the mapped excised specimen; the white straight line segments are normal epithelium (squamous or immature metaplasia); black lines indicate no epithelium or burned epithelium; red lines are HSIL and blue lines are LSIL.

The location of acetowhite epithelium and the anatomical sites detected by the image analysis system has been evaluated using one colposcopist's annotation as the criterion standard. The true positive and true negative results are computed based on pixel-to-pixel match (number of overlapping pixels) between the result of the automated image analysis system and the colposcopic annotations. A positive percent agreement (PPA) and a negative percent agreement (NPA) can, thus, be computed for each patient to evaluate the agreement between computer detected results with the colposcopic annotation:

$$\mathrm{PPA} = \frac{N_{\mathrm{TruePositive}}}{N_{\mathrm{TruePositive}} + N_{\mathrm{FalseNegative}}}, \tag{11}$$

$$\mathrm{NPA} = \frac{N_{\mathrm{TrueNegative}}}{N_{\mathrm{TrueNegative}} + N_{\mathrm{FalsePositive}}}. \tag{12}$$

For a subset of the patients with colposcopic annotations (53 subjects), average PPA and NPA were computed for the cervix region, cervical os region, columnar epithelium, and acetowhite epithelium (Table 1). The highest PPA is noted for identification of the cervix and the lowest for identifying the cervical os. All NPA results were 90% or greater.

Figure 9 indicates the correlation between disease and the opacity indices extracted from cervical images using 99 human subjects. Ninety-two patients were given a final study diagnosis based on the most severe histology results. Seven subjects had no tissue specimen taken and for these subjects, the colposcopic diagnoses were used as criterion standard. In Fig. 9, "+" indicates normal or low-grade lesions including NED (no evidence of disease), HPV subclinical change, and CIN1, CIN12 lesions; "□" indicates high-grade lesions including CIN2, CIN23, and CIN3 lesions; and "○" indicates microinvasive or invasive cancer. The "◇" sign in the figure indicate false positives of opacity index introduced by a white-yellowish secretion called mucus. The appearance of mucus mimics the appearance of the acetowhite epithelium and causes high opacity values. The study protocol specified the removal of the mucus prior to acquiring an image but for a few subjects the mucus was not removed or additional mucus was being secreted during exam. Except the false positives introduced by mucus, from Fig. 9, we can see that normal and low-grade lesions have much lower opacity ($<5\%$) than high-grade lesions and cancer cases.

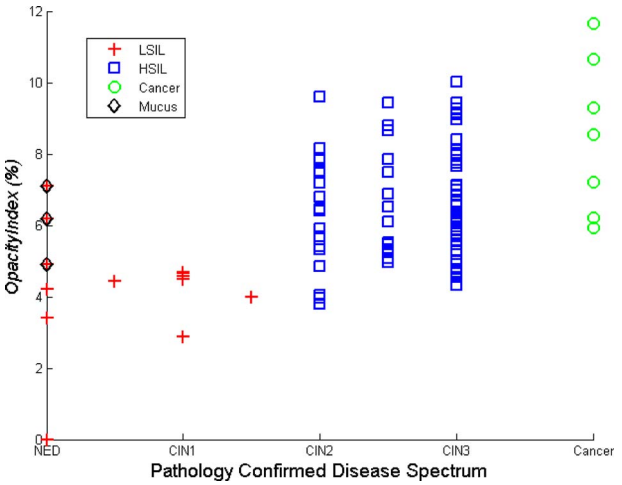

Fig. 9 Correlation between opacity index and disease spectrum of 99 human subjects.

The pathology disease spectra with corresponding opacity indices were used to populate a statistical model for classification of patients into categories of high-grade disease or non-high-grade disease. A multivariate discriminate analysis[33] was employed. Two training and testing strategies were used. One strategy was the leave-one-out method in which each subject is removed sequentially from the data set; the classifier is trained on all the remaining subjects, and the extracted subject is then predicted and compared with the pathologic findings. This procedure is repeated for all subjects. In the second strategy, the data set was randomly partitioned into five disjoint subsets (5-Folds). Four subsets were used for training, and the last subset was used for evaluation. This process was repeated five times, leaving a different subset for evaluation each time. The process for both methods was repeated 500 times respectively and the corresponding best-fit receiver operating characteristic (ROC) curves were determined, as illustrated in Fig. 10. In our application, the leave-one-out strategy produced better performance than 5-Fold according to their areas under the ROC curves (AUC). The AUC for leave-one-out was 0.94 and the AUC for 5-Fold was 0.89. The best algorithm performance in leave-one-out was 94% sensitivity and 87% specificity. Figures 9 and 10 indicate that a continuous, quantified opacity index has a high-correlation in discriminating high-grade lesions from low-grade lesions and can serve as one major diagnostic feature in a CAD system.

4 Discussion and Conclusions

Visual appraisal of the lower genital tract is a complex task. The visualization process first involves identification of the normal anatomy, when present, including epithelial and vascular features. Then, a colposcopist must differentiate normal from abnormal findings. To further entangle matters, each appraisal is unique due to substantial intrapatient variability. It is even more challenging when the evaluation is made on a static, 2-D image with varied illumination, solitary magnifica-

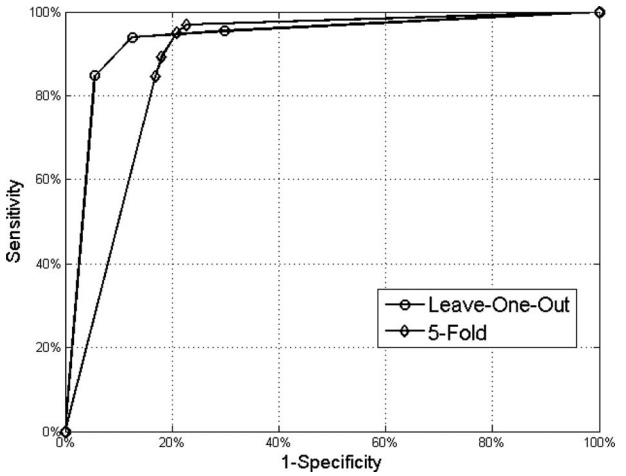

Fig. 10 ROC curves for discriminating high-grade (CIN2 and above) lesions from normal and low-grade lesions using opacity indices.

tion, fixed acetic acid response, and obscuring artifacts. The interobserver agreement in the visual evaluation of cervical images among colposcopist is, thus, low.[34,35]

The major accomplishment of this study is the potential usage of the proposed opacity index for discriminating cervical intraepithelial neoplasia and the fully automated acetowhite epithelium analysis system using two cervical images per exam. One image is taken before the acetic acid application, and the other is taken after the acetic acid application. The image analysis system first identifies the normal anatomy, including cervix, os, and columnar epithelium. Second, a texture and color analysis of the acetowhite epithelium is done using the post-acetic-acid image. Third, the pre-acetic-acid image and post acetic acid image are automatically aligned using an elastic image registration algorithm. Then, the opacity region can be extracted by subtracting the aligned pre-acetic-acid image from post-acetic-acid image and the opacity index is then computed.

Preliminary results on 99 human subjects demonstrate a high correlation of disease severity with the acetowhite opacity index. In the future, a set of algorithms can be combined with automated analyses of other cervical features such as abnormal blood vessels[36] and lesion margin characteristics[37] to derive a clinical diagnosis. We are currently scheduling large-scale clinical trials to acquire more human subject data to further evaluate and expand our system. Furthermore, the algorithms could be embedded to a screening device that can be operated by nonmedical personnel. Such a device with diagnostic capability has the potential to screen women living in locations where routine Pap testing is not possible and underserved women in developing countries where access to skilled colposcopists is limited.

There were several limitations of our study. First, the dense mucus retained on the tissue will affect the opacity index extraction and it must be excluded in advance. We are currently investigating using the motion information to detect a mucus areas through a low-resolution decay video stream. Second, the disease prevalence in our data is relative high and we require more normal and low-grade subjects to further validate our findings. However, the automated acetowhite epithelium analysis supports additional work, adding other cervical features-such as mosaic and punctation vessels. A complete system could be a valuable resource and adjunct to help reduce the morbidity and mortality associated with cervical neoplasia.

Acknowledgments

The research was partially supported by U.S. Army Medical Research and Material Command under Contract No. W81XWH-07-C-0006. The views, opinions, and/or findings contained in this paper are those of the authors and should not be construed as an official Department of the Army position, policy, or decision unless so designated by other documentation. In the conduct of research where humans are the subjects, the investigators adhered to the polices regarding the protection of human subjects as prescribed by Code of Federal Regulations Title 45, Volume 1, Part 46; Title 32, Chapter 1, Part 219; and Title 21, Chapter 1, Part 50 (Protection of Human Subjects). The authors would like to thank Instituto Especializado de Enfermedades Neoplasicas (INEN), Lima, Peru, for data acquisition, and Jan Kybic at Center for Machine Perception, Czech Technical University, Prague, for collaboration on image registration. The authors would also like to thank the reviewers for their valuable suggestions and comments.

References

1. D. Ferris, J. T. Cox, D. M. O'Connor, V. C. Wright, and J. Foerster, *Modern Colposcopy, Textbook and Atlas*, American Society for Colposcopy and Cervical Pathology, Dubuque, IA (2004).
2. R. Reid and P. Scalzi, "Genital warts and cervical cancer. VII. An improved colposcopic index for differentiating benign papillomaviral infections from high-grade cervical intraepithelial neoplasia," *Am. J. Obstet. Gynecol.* **153**, 611–618 (1985).
3. J. T. Cox, M. Schiffman, and D. Solomon, "Prospective follow-up suggests similar risk of subsequent cervical intraepithelial neoplasia grade 2 or 3 among women with cervical intraepithelial neoplasia grade 1 or negative colposcopy and directed biopsy," *Am. J. Obstet. Gynecol.* **188**, 1406–1412 (2003).
4. S. Yang, J. Guo, P. King, Y. Sriraja, S. Mitra, B. Nutter, D. Ferris, M. Schiffman, J. Jeronimo, and R. Long, "A multi-spectral digital cervigram?analyzer in the wavelet domain for early detection of cervical cancer," *Proc. SPIE* **5370**, 1833–1844 (2004).
5. S. Gordon, G. Zimmerman, and H. Greenspan, "Image segmentation of uterine cervix images for indexing in PACs," in *Proc. IEEE 17th Symp. on Computer-based Medical Systems*, pp. 298−303 (2004).
6. S. Gordon, G. Zimmerman, R. Long, S. Antani, J. Jeronimo, and H. Greenspan, "Content analysis of uterine cervix images: initial steps towards content based indexing and retrieval of cervigrams," *Proc. SPIE* **6144**, 1549–1556 (2006).
7. B. W. Pogue, M. A. Mycek, and D. Harper, "Image analysis for discrimination of cervical neoplasia," *J. Biomed. Opt.* **5**, 72–82 (2000).
8. B. W. Pogue, H. B. Kaufman, A. Zelenchuk, W. Harper, G. C. Burke, E. E. Burke, and D. M. Harper, "Analysis of acetic acid-induced whitening of high-grade squamous intraepithelial lesions," *J. Biomed. Opt.* **6**, 397–403 (2001).
9. C. J. Balas, G. C. Themelis, E. P. Prokopakis, I. Orfanudaki, E. Koumantakis, and E. S. Helidonis, "In vivo detection and staging of epithelial dysplasias and malignancies based on the quantitative assessment of acetic acid-tissue interaction kinetics," *J. Photochem. Photobiol., B* **53**, 153–157 (1999).
10. C. Balas, "A novel optical imaging method for the early detection, quantitative grading, and mapping of cancerous and precancerous lesions of cervix," *IEEE Trans. Biomed. Eng.* **48**, 96–104 (Jan. 2001).
11. H. Kaufman, A. Zelenchuk, R. Flewelling, P. Schmid, and Z. Hed, "Methods of monitoring effects of chemical agents on a sample," U.S. Patent No. 6,902,935 B2 (June 7, 2005).

12. S. Y. Park, M. Follen, A. Milbourne, H. Rhodes, A. Malpica, N. Mackinnon, C. MacAulay, M. K. Markey, and R. Richards-Kortum, "Automated image analysis of digital colposcopy for the detection of cervical noplasia," *J. Biomed. Opt.* **13**, 014029-1–014029-10 (2008).
13. W. Li, M. Soto-Thompson, and U. Gustafsson, "A new image calibration system in digital colposcopy," *Opt. Express* **26**, 12887–12901 (Dec. 2006).
14. R. C. Gonzalez and R. E. Woods, *Digital Image Processing*, Prentice-Hall, Upper Saddle River, NJ (2002).
15. G. Van de Wouwer, P. Scheunders, S. Livens, and D. Van Dyck, "Wavelet correlation signatures for color texture characterization," *Pattern Recogn.* **32**, 443–451 (1999).
16. S. A. Karkanis, D. K. Iakovidis, D. E. Maroulis, D. A. Karras, and M. Tzivras, "Computer-aided tumor detection in endoscopic video using color wavelet features," *IEEE Trans. Inf. Technol. Biomed.* **7**, 141–152 (2003).
17. A. Dempster, N. Laird, and D. Rubin, "Maximum likelihood from incomplete data via the EM algorithm," *J. R. Stat. Soc. Ser. B (Stat. Methodol.)*, **39**, 1–38 (1977).
18. Wikipedia, "Expectation-maximization algorithm," http://en.wikipedia.org/wiki/Expectation-maximization_algorithm.
19. S. Venkataraman and W. Li, "Improving cervical region of interest by eliminating waginal walls and cotton swabs for automated image analysis," *Proc. SPIE* **6914**, 69143E-1–69143E-8 (2008).
20. K. Fukunaga and L. D. Hostetler, "The estimation of the gradient of a density function, with applications in pattern recognition," *IEEE Trans. Inf. Theory* **21**, 32–39, (1975).
21. D. Comaniciu and P. Meer, "Mean shift: a robust approach toward feature space analysis," *IEEE Trans. Pattern Anal. Mach. Intell.* **24**, 603–619 (May 2002).
22. R. Fabbri, L. D. F. Costa, J. C. Torelli, and O. M. Bruno, "2D Euclidean distance transforms: a comarative survey," *ACM Comput. Surv.* **40**, 2-1–2-41 (2008).
23. Wikipedia, "Distance Transform," http://en.wikipedia.org/wiki/Distance_transform.
24. W. Forstner, "A framework for low level feature extraction," in *Proc. Eur. Conf. on Computer Vision*, pp. 383–394 (1994).
25. J. Grading and T. Lindeberg, "Direct computation of shape cues using scale-adapted spatial derivative operators," *Int. J. Comput. Vis.* **17**, 163–191 (Feb. 1996).
26. C. Carson, S. Belongie, H. Greenspan, and J. Malik, "Blobworld: image segmentation using expectation-maximization and its application to image querying," *IEEE Trans. Pattern Anal. Mach. Intell.* **24**, 1026–1038 (Aug. 2002).
27. W. Li, J. Gu, D. Ferris, and A. Poirson, "Automated image analysis of uterine cervical images," *Proc. SPIE* **6514**, 65142P-1–65142P-9 (2007).
28. G. Paschos, "Perceptually uniform color spaces for color texture analysis: an empirical evaluation," *IEEE Trans. Image Process.* **10**, 932–936 (June 2001).
29. T. Kanungo, D. M. Mount, N. Netanyahu, C. Piatko, R. Silverman, and A. Y. Wu, "An efficient k-means clustering algorithm: analysis and implementation," *IEEE Trans. Pattern Anal. Mach. Intell.* **24**, 881–892 (2002).
30. G. Yang, C. V. Stewart, M. Sofka, and C.-L. Tsai, "The generalized dual-bootstrap ICP algorithm with application to registering challenging image pairs," *IEEE Trans. Pattern Anal. Mach. Intell.* **22**, 1379–1394 (2008).
31. J. D. Garcia-Arteaga, J. Kybic, and W. Li, "Elastic image registration for movement compensation in digital colposcopy," in *Proc. 18th Int. EURASIP Conf. BIOSIGNAL*, pp. 236–238, EURASIP (2006).
32. J. Kybic and M. Unser, "Fast parametric elastic image registration," *IEEE Trans. Image Process.* **12**, 1427–1442 (Jan. 2003).
33. W. J. Krzanowski, *Principles of Multivariate Analysis*, Oxford University Press, New York (1988).
34. D. G. Ferris and M. Litaker, "Interobserver agreement for colposcopy quality control using digitized colposcopic images during the ALTS trial," *J. Low. Genit. Tract Dis.* **9**, 29–35 (Jan. 2005).
35. J. Jeronimo, L. S. Massad, P. E. Castle, S. Wacholder, and M. Schiffman, "Interobserver agreement in the evaluation of digitized cervical images," *Obstet. Gynecol. (N.Y., NY, U. S.)* **110**, 833–840 (Oct. 2007).
36. W. Li and A. Poirson, "Detection and characterization of abnormal vascular patterns in automated cervical image analysis," *Lect. Notes Comput. Sci. Adv. Vis. Comput.* **4292**, 627–636 (Nov. 2006).
37. W. Li, V. Van Raad, J. Gu, U. Hansson, J. Hakansson, H. Lange, and D. Ferris, "Computer-aided diagnosis (CAD) for cervical cancer screening and diagnosis: a new system design in medical image processing," *Lect. Notes Comput. Sci. CVBIA 2005*, **3795**, 240–250 (2005).